International Astronomy and Astrophysics Research Journal

2(1): 1-12, 2020; Article no.IAARJ.53022

Observations of Inertial-gravity Waves Observed from Long-lasting Meteor Trail Echoes

M. Satyavani[1], P. S. Brahmanandam[2*], P. S. V. Subba Rao[3], C. T. Cheng[1] and Y. H. Chu[1]

[1]Department of Physics, Andhra University, Visakhapatnam - 530 003, India.
[2]Department of Basic Science, Shri Vishnu Engineering College for Women, Bhimavaram - 534 202, India.
[3]Institute of Space Science, National Central University, Chung-Li, Taiwan, R.O.C.

Authors' contributions

This work was carried out in collaboration among all authors. Authors PSB and CTC designed the study, performed the statistical analysis, wrote the protocol and wrote the first draft of the manuscript. Authors MS and YHC managed the analyses of the study. Author PSVSR managed the literature searches. All authors read and approved the final manuscript.

Article Information

Editor(s):
(1) Dr. Rachana Pathak, Assistant Professor, Faculty of Engineering, University of Lucknow, Lucknow, India.
(2) Dr. Hadia Hassan Selim, Professor, Department of Astronomy, National Research Institute of Astronomy and Geophysics, Cairo, Egypt.
Reviewers:
(1) Sie Long Kek, Universiti Tun Hussein Onn Malaysia, Malaysia.
(2) Abhik Kumar Sanyal, University of Kalyani, India.
(3) Francisco Bulnes, Tecnológico de Estudios Superiores de Chalco, Mexico.
(4) Mihai Todica, "Babes-Bolyai" University, Romania.
(5) Özlem Yeşiltaş, Gazi University, Turkey.
Complete Peer review History: http://www.sdiarticle4.com/review-history/53022

Original Research Article

Received 02 November 2019
Accepted 08 January 2020
Published 11 January 2020

ABSTRACT

Horizontal background wind in the mesosphere and lower thermosphere region of the Earth's atmosphere deduced from the temporal displacement of a long- lasting meteor trail was estimated and investigated in this paper. The meteor trail echoes lasting more than 23 seconds in height range between 95 and 108 km as measured using the interferometry technique implemented at the Chung-Li 52 MHz radar, Chung-Li, Taiwan. The 3-meter electron density irregularities embedded in the meteor trail, which were responsible for the radar returns, were found without field-aligned property. Hodograph analysis reveals that the existence of an upward propagating inertia-gravity

**Corresponding author: E-mail: dranandpotula@svecw.edu.in;*

wave is associated with the vertical wavelength of 11.3 km. The wave-induced wind velocity and temperature perturbations combined with the background temperature profile of mass spectrometer and incoherent scatter (MSIS) model was used to estimate the height variation of the Richardson number (R_i). It is found that the feature $R_i < 0.25$ occurred in height range from 98 to 99 km, which implies that the wave is very likely broken in this height region through convective instability that was associated with negative temperature gradient induced by the gravity wave. The characteristics of echo power and spectral width associated with the wave-breaking turbulences are also discussed.

Keywords: Mesosphere and lower thermosphere; 52 MHz Chung-Li very high frequency radar; meteors; MSIS model.

1. INTRODUCTION

It has long been recognized that the upward propagating inertia gravity waves generated in the lower atmosphere play important roles in changing the background mean flow of the middle atmosphere through the wave breaking process that transports the wave momentum and energy to the mean flow [1]. Theoretical studies have observed various aspects of gravity wave characteristics [2,3]. When the period of a gravity wave is comparable to the inertial period, it is called an inertia gravity wave. The intrinsic frequency, vertical and horizontal wavelengths are three main characteristic parameters to classify different waves as a planetary wave, diurnal tide and gravity wave. There are other parameters like propagating direction, amplitude, and phase which can be used to track how a gravity wave propagates and breaks down in the Earth's atmosphere. Several experimental techniques including in -situ measurements of meteor trail made with a sounding rocket [4], ground-based radar [5-8] and lidar observations [9,10], and passive airglow photometers [11] have been employed to observe the characteristics of gravity waves [12,10,13,14].

For example, by using lidar observations Dao et al. [10] found the evidence of mesopause heating which related to the diurnal activity based on the downward progression of the perturbations and the observed temperature fluctuations were associated with a long period gravity wave. By comparing the observations of mesospheric gravity waves by the middle and upper atmosphere (MU) radar located in Kyoto, Japan, and the sodium lidar, Namboothiri et al. [9] have found the dominant gravity wave along with its characteristics. The meteor echo observations data of MU radar were applied to detect mesospheric gravity waves and the result showed an upward propagating wave with a vertical wavelength of around 16 km, the intrinsic period of 9.1 hours, and horizontal wavelength of 1900 km. Chu et al. [14] found evidence on a vertically propagating inertio-gravity wave with a period of 11.2 hr and a vertical wavelength of 19.5 km in the height range 98.5–122.0 km with a sounding rocket Trimethyl aluminum (TMA) release experiment.

As far as the applicability of this research is concerned, it has been well known for the last three decades that the momentum deposition arising from the dissipation of atmospheric gravity waves has a major influence on the background wind and thermal structure of the mesosphere– lower- thermosphere / ionosphere (MLT/I; ∼80–100 km altitude) [15,16]. The small scales of the gravity waves (GWs) relative to typical grid spacing in global climate models (GCMs) have led to a need to incorporate accurate parameterizations of the gravity wave (GW) forcing within the GCMs [17,18].

The range spread echoes cannot be interpreted as the radar returns reflected from the meteor trails with the axes normal to the radar wave vectors, which is expected to occur only in a specific range bin. Chapin and Kudeki [19] suggested that the strong discharge current in the meteor trail may result in sufficient large electron drift velocity to excite two-stream and/or gradient drift instabilities to account for the generations of 3-meter plasma irregularities responsible for the range spread echoes. Reddi and Nair [20] interpreted the range spread echoes as the radar waves reflected from the striations produced along the meteor trail parallel to the geomagnetic field.

The meteor trail is cylindrical and typically kilometres in length and meters in diameter. The duration of the ionized meteor trails will vary and few trails can last many seconds [21]. The observed spatial drift of the long-lasting meteor trail echo in this paper provides background wind

field very well around 100 km attitude, where vary few techniques can measure wind velocities. From the frozen-in assumption, we can treat that meteor plasma trail variation is dominated by background wind field and estimate characteristics of gravity through the hodograph analysis. Because of meteor radar echoes can be detected all day, it is a great advantage for mesospheric gravity research. Especially, the long duration meteor trail echo event can help us to understand the evolution of gravity wave propagating through the mesosphere.

In this paper, we will describe the results of the hodograph analysis and determine an upward propagating gravity wave. Later, we will introduce the experimental setup of Chung-Li very high frequency (VHF) radar and the preliminary procedures of data analysis. In section 3, the theory of hodograph analysis will be expounded and we will demonstrate polarization and dispersion relations of linear gravity wave. The discussion of the simultaneous data and the possible wave-breaking source are both presented in section 4. The conclusion is drawn in section 5.

2. EXPERIMENTAL RESULTS

2.1 Experimental Setup and Data Analysis

A long-lasting meteor trail echo studied in this paper was observed by the 52 MHz Chung-Li VHF radar on August 8, 1997, from 03:37:44 to 03:38:09 LT. The radar parameters employed for the observation were set as follows: 70 kW of peak transmitted power, 28 μs of pulse length with 7-bit Barker code, 2 ms of the inter-pulse period, and 123.6 -159 km range coverage for echo detection. Three independent antenna array modules were operated simultaneously to detect the echoes so that the spatial domain interferometry measurement can be conducted to locate the positions of the targets in the echoing region. The half- power beamwidths of each antenna array module were 7.5° in elevation and 15° in azimuth directions, respectively. The antenna beam axis was pointed in a fixed direction of 22.3° west of geographic north at a zenith angle of 41°. Fig. 1 presents the range-time-intensity (RTI) plot of the meteor trail echoes that lasted more than 25 seconds in the range extent of 131-154 km. As shown, prominent meteor head echoes were observed at the leading edge of the long- lasting echoes, which was characterized by a sharp range rate and strong echo intensity with a very short duration (about 0.4 sec). Because the main theme of this article focuses on the analysis of long-lasting meteor echoes to study inertia-gravity wave propagating in Mesosphere and Lower Thermosphere (MLT) region, the head echoes were excluded in the data analysis to avoid plausible impairment on the background wind velocity estimation.

In light of limitation of the relatively short duration of the measured meteor trail echoes, the use of Fourier transform method is an inappropriate means to collect sufficient phase information to position the location of the meteor trail in the echoing region in terms of interferometry technique in the spatial domain [22,23]. We, therefore, apply the cross-correlation analysis method to each pair of the time sequence of the meteor trail echoes for range bins from 16 to 39 (corresponding to range extent 96-109 km) to estimate their phase differences for the location positioning. In the practical data processing, we employed 100 raw data points to calculate the complex cross-correlation function and its phase around zero lag was adopted for interferometry analysis.

Fig. 2 shows an example of the spatial distribution of the meteor trail projected on vertical to zonal planes for period 03:37:46-03:38:08. For the Chung-Li VHF radar, the echo patterns projected on the vertical plane, which are generated from 3-m field-aligned electron density irregularities, should occur within this angular range [23]. It is noteworthy to point out that, if the electron density fluctuations embedded in the meteor trail are field-aligned, only very small portion of the entire meteor trail that locates at the place where the radar wave vector is approximately perpendicular to the local magnetic field line can be resolved by the radar [24]. In this case, it is unlikely to reconstruct the whole configuration of the meteor trail in terms of the interferometry method. Furthermore, the corresponding echo pattern projected on the vertical plane is expected to distribute along a line with an elevation angle between 49° and 52° [24].

However, as shown in Fig. 2, in spite of most of the meteor echoes were in the sporadic E region, the distribution of the echo pattern from the meteor trail was not in the region with the field-aligned property. Under above- said conditions, the estimation of the background wind velocity from the displacement of the meteor trail echoes to study the property of a gravity wave propagating to a large height extent is possible.

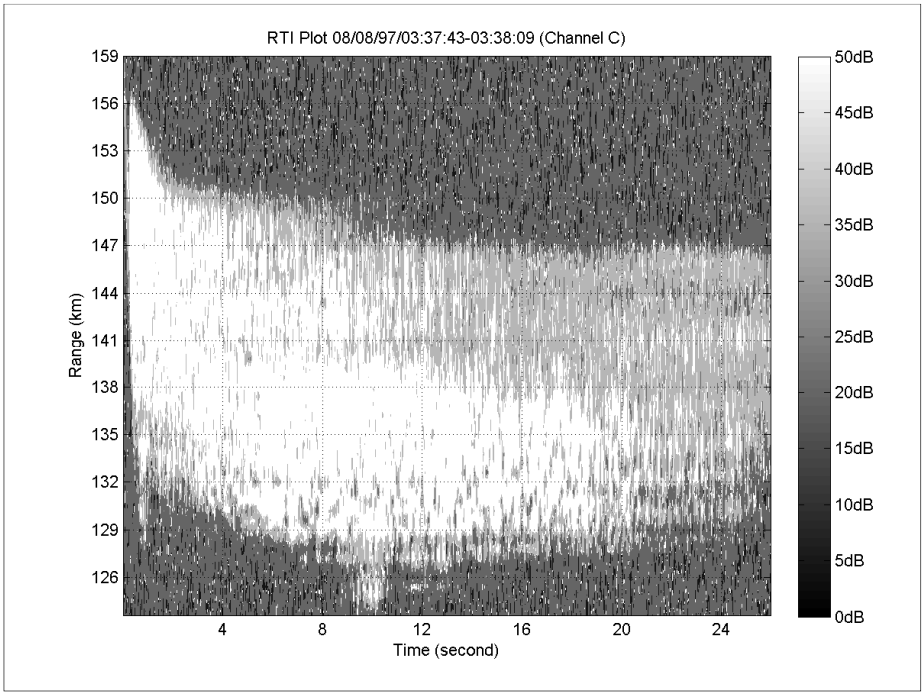

Fig. 1. The range-time-intensity contour plot of the radar returns from meteor echo recorded by channel c of the Chung-Li VHF radar

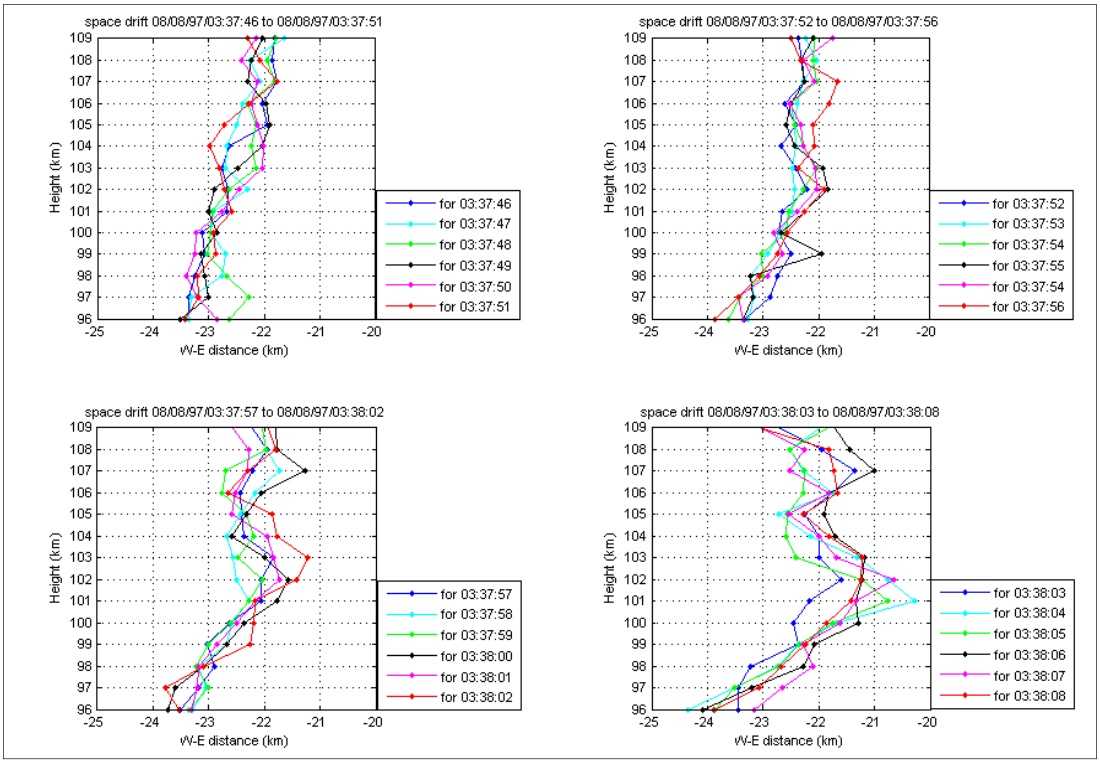

Fig. 2. The east-west direction spatial distribution of the echoing altitudes (96-109 km) for meteor trail in the period 08/08/1997 03:37:46-08/08/1997 03:38:08 LT. The six different colors stand for each different time

Fig. 3 shows the time sequence of the meteor trail projected on vertical to meridional planes, in which each profile represents the mean location of the meteor trail per second in period 03:37:46-03:38:08. As shown in the azimuth and vertical planes, continuous changes in the horizontal locations of the meteor trail profile in height ranges 99-103 km and 96-97 km were clearly observed. This feature provides direct evidence showing the existence of strong background wind velocities in these two height ranges. In addition, relatively indistinct displacements of the meteor trail with time in other height ranges are seen as well, suggesting weak wind velocities there.

Fig. 4 presents averaged profiles of the wind velocity components in the zonal (solid curve) and meridional (dashed curve) directions during the period from 03:37:43 to 03:38:09 LT. As shown, very intense wind velocities with a magnitude of about 95 m/s occurred at heights around 96 and 102 km. From the height variation in the horizontal wind velocity, it appears that the vertical wavelength of the wind velocity is about 11 km. The implication of the quasi-periodic oscillation of the horizontal wind velocity is the presence of a large scale gravity wave propagating in the vertical direction. The characteristics of the wave propagation can be obtained from the hodograph analysis and that will be presented in the ensuing sections.

3. HODOGRAPH ANALYSIS

In this section, the hodograph method combined with polarization and dispersion relations of a linear gravity wave is employed to analyze the horizontal wind profile in order to estimate the parameters of the gravity wave that dominated the spatial structure and dynamic behavior of the meteor trail. When an inertia-gravity wave propagates upward in the atmosphere with a uniform background wind field, its corresponding polarization equation is given by Gossard and Hooke [25].

$$U = \frac{wk + i2\Omega_z l}{wl - i2\Omega_z k} V \qquad (1)$$

where U and V are, respectively, eastward and northward components of horizontal wind velocity, ω is intrinsic wave frequency, Ω_z *(=Ωsinψ)* is component of earth's angular velocity (=7.292) in local zenith direction, ψ is latitude of location, k and l are, respectively, the wave vector components in zonal and meridional directions. With an angle α which is determined *by*$\alpha = \tan^{-1}(l/k)$, we rotate the coordinate system of U and V and Equation (1) is reduced to

$$\frac{u}{v} = \frac{iw}{2\Omega_z} \qquad (2)$$

where u and v are, respectively, the horizontal perturbation velocities parallel and perpendicular to the wave propagation direction. Note that the amplitudes of u and v are corresponding to the major and minor axes of hodograph ellipse.

From Equation (2), for an upward propagating gravity wave, the horizontal wind vector will trace out an ellipse that rotates in a clockwise sense with the increase of height with the major axis aligned in the horizontal direction of the wave propagation. Moreover, the ratio of major to minor axes of the ellipse is equal to ω/2Ωz and the intrinsic frequency can be estimated from this ratio in accordance with (2). On the base of the hodograph of the horizontal wind vector, the wave characteristics, such as intrinsic frequency, horizontal wavelength, the amplitude of wave perturbation, wave propagation direction, etc., are capable of being estimated in accordance with the polarization and dispersion relations of the inertia-gravity wave. Fig. 5 shows the hodograph of the wind velocity, in which the ellipse (solid curve) is the best fit to the observed data (open circle). As illustrated, the horizontal winds rotate clockwise with height and the loci of the wind vectors can be well described by a tilted ellipse with major axis oriented in the north-west and south-east (NW-SE) direction at an acute angle of about 45° with respect to the west direction. This result implies that a quasi-monochromatic gravity wave propagated upward in this height range and dominated the background wind field. A number of gravity wave parameters can be directly scaled from the hodograph ellipse as shown in Fig. 5.

The center of the ellipse represents the mean state wind velocity that will cause the Doppler Effect on observed wave frequency. The vertical wavelength (about 11.3 km) can be estimated from the revisited height of the ellipse. The major and minor axes of the ellipse are, respectively, indicative of amplitudes of wind velocity perturbations in the directions of parallel and perpendicular to the horizontal wave propagation direction that can be read from the tilted angle of the major axis of the ellipse. From the ratio of the major to minor axes as shown in Fig. 5, the

intrinsic wave period is estimated to be about 6 hours for the present wave event. Moreover, the horizontal wavelength λ_h is able to be obtained by substituting vertical wavelength and intrinsic wave frequency into gravity wave dispersion relation that is given by Gossard and Hooke [25]

$$n^2 = \frac{N^2 - w^2}{w^2 - 4\Omega_z^2} m^2 + \frac{w^2}{c_s^2} - \frac{1}{4H^2} \quad (3)$$

where n (=2π/λ_h) and m (=2π/λ_v) are, respectively, vertical and horizontal wavenumbers, N is the Brunt-Vaisala frequency *(=gdlnθ/dz)*, θ is potential temperature, g is gravity acceleration, c_s is sound speed, and H is the scale height *(=KT/mg)*. The MSIS-E 90 model is employed to calculate background values of N and H in the height region (95-110 km) where the meteor trail echoes occurred [26].

Fig. 6 shows the profiles of scale height, Brunt-Vaisala frequency and sound speed over Taiwan in August, which are computed form MSIS-E 90 model with g=9.5 m/s^2 which is the mean value of gravity acceleration in height range 90-110 km. As shown in Fig. 6, the Brunt-Vaisala frequency is in the range 0.0203-0.0286 rad/s. Substituting the mean values of measured λ_z *(=11.3 km), ω (=1.5×10^{-4} rad/s)*, N (about 0.0249 rad/s), Cs (about 309 m/s), and H (5.7 km) in the height range 90-110 km into Equation (3), we obtain the horizontal wavelength (λ_h) is about 1038 km. The characteristics of the inertia-gravity wave deduced from hodograph analysis, including vertical wavelength λ_z, horizontal wavelengthλ_h, intrinsic wave period, possible wave propagation direction and horizontal perturbation velocity to the wave propagation direction in horizontal u, are summarized in Table 1. Note that, because of lacking sufficient information, such as perturbations of temperature and vertical wind velocity of the gravity wave, the exact horizontal wave propagation direction cannot be determined from single a profile of the horizontal wind field.

Fig. 7 presents the vertical profiles of wind shears and the Richardson numbers, respectively, in the height region from 97 km to 106 km from the data of real- time. In Fig. 7, the red line in the right subfigure is the Richardson numbers equal to 0.25 and there are two regions below the 0.25 threshold. These two height regions with less than 0.25 values of the Richardson numbers are, respectively, 98-99 km and 103-104 km.

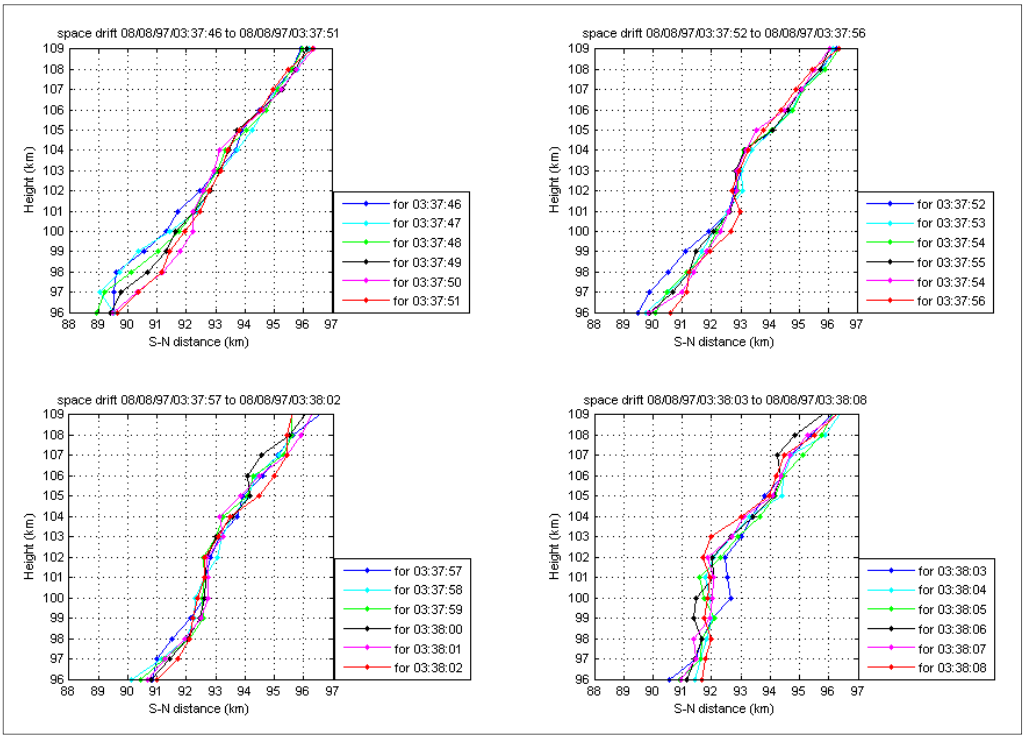

Fig. 3. Same as Fig. 2, but for the south-north direction

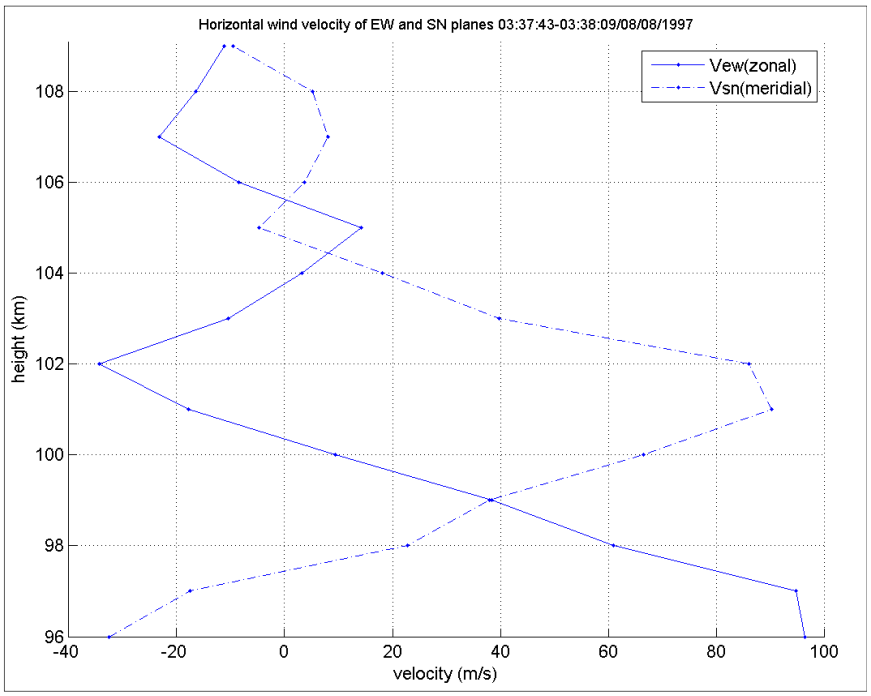

Fig. 4. The zonal and meridional wind field in the height region of 96 km to 109 km, where continuous blue line is the zonal wind velocity and the dotted blue line is the meridional wind velocity

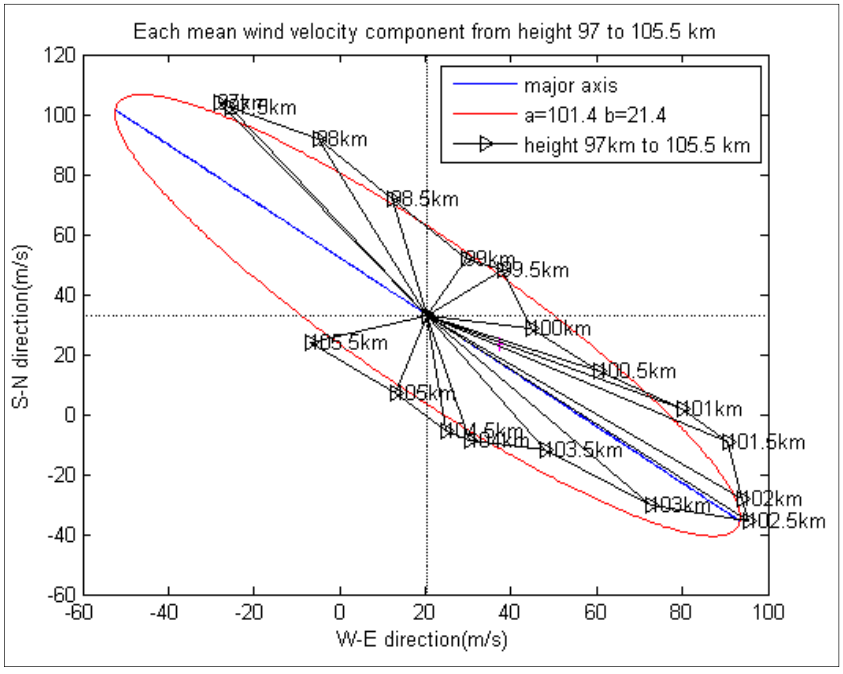

Fig. 5. The hodograph in the altitude regions 97 km to 105.5 km obtained from 03:37:43 to 03:38:09 LT on August 8, 1997, where the black dot line is the wind vectors and the red ellipse is a fitting result

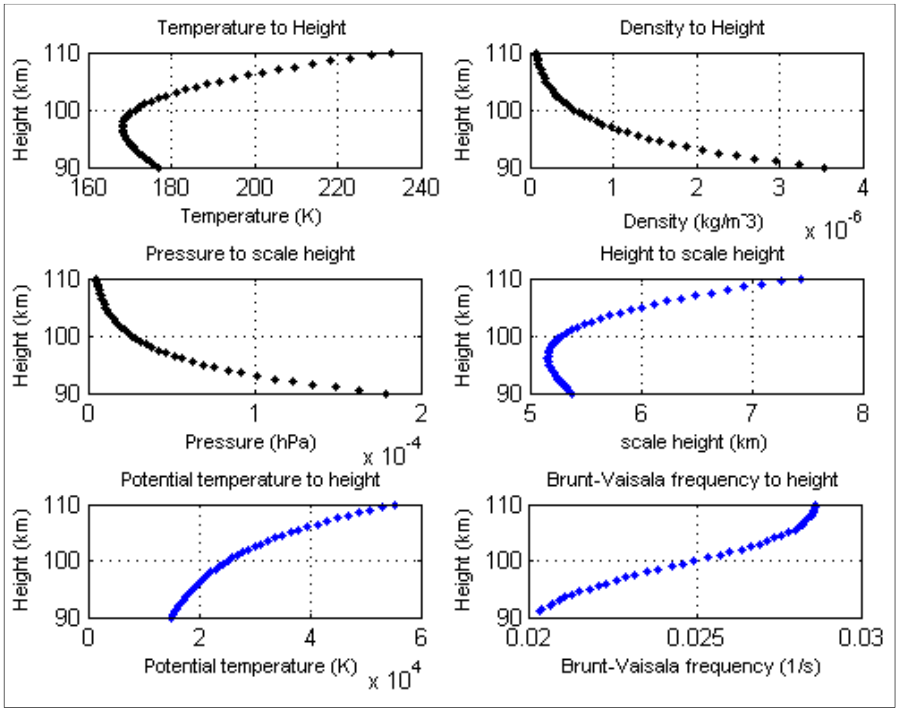

Fig. 6. The MSIS simultaneous data of temperature, density and pressure varying with heights from 90 km to 110 km and the calculated data of scale height, potential temperature and Brunt-Vaisala frequency correspond to heights from 90 km to 110 km

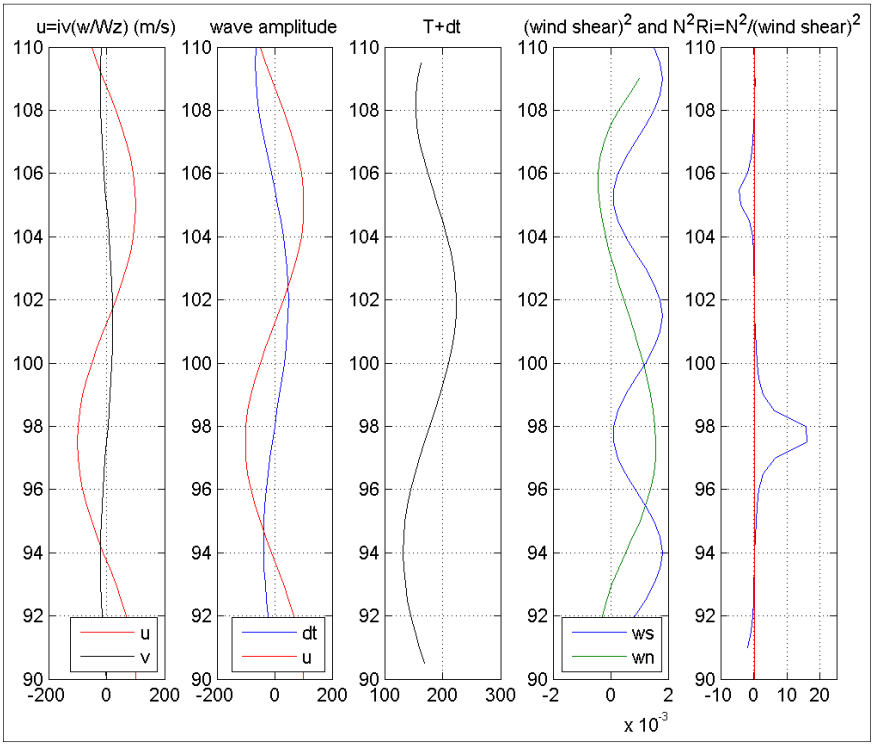

Fig. 7. The gravity wave simulation result from hodograph analysis and the Richardson number R_i calculated from wind shear

Table 1. The gravity wave parameters obtained from the hodograph analyses of height profile of meteor wind velocity observed with the Chung-Li VHF Radar on August 8, 1997

Vertical wavelength (λ_z), km	Horizontal wavelength (λ_h), km	Wave period, hours	Propagation direction, deg	Major axis of ellipse (u), m/s	Minor axis of ellipse (v), m/s	Center of ellipse, m/s
11.3	1038	6.0	225^0 or 45^0	101.4	21.4	(20.5, 32.9)

4. DISCUSSION

It is to be noticed that the hodograph ellipse fitting is based on nearly 3/4 cycle phase of wave propagation and it is likely a wave breaking effect. Thus the polarization did not get a full cycle pattern. The polarization and dispersion relations that we apply to hodograph analysis were derived from the assumed linearized equations which are probably not fully usable in the non-linear wave breaking process and we will discuss the wave breaking process of this event in future research.

Inspecting Fig. 1 in more detail shows that salient meteor head echoes lasting about 0.4 seconds were observed in range extent 135.6-159.6 km, which is characterized by straight line-like echo pattern with enormously large range rate (about 51 km/s for the present case) in range-time-intensity plot. Note that the meteor head echoes are primarily generated from the scattering of the dense ionized region surrounded the meteoroid [27]. Because of this, the estimated range rate of the meteor trail echoes that is to some degree indicative of the falling velocity of the meteoroid is computed from the slant range with respect to the radar and, therefore, expected to be greater than the real falling velocity of the meteor head relative to the Earth center. In addition, it is noteworthy that the estimated range rate is slightly different from the actual meteoroid falling velocity. Especially notice from Fig. 1 that the head echoes seemed to be immediately followed by the meteor trail echoes and no discernible time delay between them was observed.

According to the theory of Oppenheim et al. [28], a time delay between head echo and trail echo is expected if the gradient drift/Farley Buneman instabilities are responsible for the excitation of 3-meter electron density irregularities in the ionized meteor trail that generate the range spread meteor trail echoes. The subsequent range spread echoes which were sampled at very high resolution (4 ms) not only bending down in ranges but also decreasing in power density. The range spread echoes followed immediately with the head echo but there is no apparent time delay between them.

The retrieved wind field and gravity wave phenomenon inside the background wind field from meteor trail echo are the first time observed over Taiwan. From the hodograph pattern, it is obvious to see that an upward propagating gravity wave turned to break around 105 km height. When a region of atmospheric instability occurs, the temperature usually disturbs and accompanied by convective or shear instability. One of the possible unstable regions is the mesosphere inversion layer, so- called MIL. The mesosphere and lower thermosphere (MLT) is from 60 to 130 km and the mesosphere inversion layer (MIL) phenomenon is linked to the turbulence generation which could cause inertial gravity wave breaking in this region. In the MLT region, two MILs are observed and one mesosphere inversion layer is around the upper mesosphere (60-70 km) and the other one is the mesopause (90-100 km). The MIL region temperature enhancement (typically 10-25 Kelvin) of the background atmosphere could be attributed to the breaking of gravity waves. When such events appeared, the region convective (or shear) instabilities usually coexist. In the MIL region, the decrease in Brunt-Vaisala frequency (N) caused by the higher temperatures reduces the atmospheric stability and the waves breaking consequently occurred. Arising from the breaking waves, the turbulent heating provides a feedback mechanism maintaining the MIL.

However, another possible source of inducing gravity wave breaking is the vertical atmospheric instability and the enormously large wind shears (convective instability) will occur in this unstable region. Convective instability occurs while the gradient of total potential temperature becomes negative i.e. Richardson number is between 0 and 1/4.

Base on the data of Fig. 5, we can calculate the vertical wind shear profile and estimate the Richardson number which is given as follows:

$$R_i = \frac{g}{T}\left(\frac{dT}{dz} + \frac{g}{c_p}\right) \Big/ \left[\left(\frac{dU}{dz}\right)^2 + \left(\frac{dV}{dz}\right)^2\right] \quad (4)$$

where U and V are, respectively, the zonal and meridional components of the horizontal wind velocity in unit m/s, g is gravity acceleration assumed as 9.5 m/s^2 in MLT region, T is atmospheric temperature in unit K adopted from MSIS-E-90, and c_p = 1004 J/K/kg is the specific heat at constant pressure. Equation (4) also can be regarded as the square of the Brunt-Vaisala frequency divided by the square of wind shear. The Richardson number determines the convective (or static) stability of the atmosphere. While vertical temperature gradient is zero or ever turning to negative, a convective instability may be induced and, at the same time, the turbulence may occur through the overturning process. The Richardson number will drop to less than 0.25 when the wind shear effect overwhelms the buoyancy effect and the dynamic instability may be excited with the turbulence. We presume that the atmospheric instability of two close regions (98-99 km and 103-104 km, according to Fig. 7) could be the dynamic source of inertia-wave breaking.

5. CONCLUSION

On the basis of a long- lasting (over 23 seconds) meteor trail echo and through the interferometry technique, the background horizontal wind field can be estimated by the averaged spatial displacement. Applying the hodograph analysis, the wind vector rotates clockwise with the increase of height and inertial gravity wave with period 6 hours exist in the height region from 96 km to 109 km. The other wave parameters are also determined by the polarization and dispersion relation of gravity wave, such as the vertical wavelength is 11.3 km, the horizontal wavelength is 1038 km, the propagation direction is oriented in south-north- west-east (SN-WE) direction at an acute angle of 45°. The wave-induced profile of Richardson number R_i is calculated from perturbations of wind velocity and temperature of the gravity wave combined with a background environment of the MSIS model.

As far as the future research is concerned, relatively low predictability of turbulence associated with convective sources is particularly problematic, and until numerical weather prediction (NWP) models are better at forecasting the timing, location, and intensity of convective storms, using short-term newscasts for tactical avoidance could be the only viable approach. Such efforts have already started and interested readers may verify the research works of Pearson and Sharman [29].

ACKNOWLEDGEMENT

This work was partially supported by National Science Council of the Republic of China in Taiwan under grant NSC97-M-2020-008-01. The corresponding author, Dr. P. S. Brahmanandam, gratefully acknowledges the Management of SVECW (Autonomous), Bhimavaram, Andhra Pradesh, India for their logistic support.

COMPETING INTERESTS

Authors have declared that no competing interests exist.

REFERENCES

1. Fritts DC, Isler JR, Andreassen O. Gravity wave breaking in two and three dimensions: 1. Three-dimensional evolution and instability structure. J. Geophys. Res. 1994;8109–8123.
2. Schoeberl MR, Strobel DF, Apruzese JP. A Numerical Model of Gravity Wave Breaking and Stress in the Mesosphere. J. Geophys. Res. 1983;5249–5259.
3. Dewan E M, Good RE. Saturation and the Universal Spectrum for Vertical Profiles of Horizontal Scalar Winds in the Atmosphere. J. Geophys. Res. 1986; 2742–2748.
4. Kelley MC, Alcala C, Cho JYN. Detection of a meteor contrail and meteoric dust in the Earth's upper mesosphere. Journal of Atmospheric and Terrestrial Physics. 1998; 359-369.
5. Oleynikov AN, Jacobi Ch, Sosnovchik DM. Parameters of internal gravity waves in the mesosphere-lower thermosphere region derived from meteor radar wind measurements. Ann. Geophys. 2005; 3431–3437.
6. Antonita TM, Ramkumar G, Kishore Kumar K, Sunil Kumar SV. Quantification of gravity wave forcing in driving the

stratospheric Quasi-Biennial Oscillation. Geophys. Res. Lett.; 2008.
DOI: 10.1029/2008GL033960.

7. Mitchell NJ, Beldon C L. Gravity waves in the mesopause region observed by meteor radar, 1: A simple measurement technique, J. Atmos. Sol. Terr. Phys., 2009, 866–874.
8. Spargo AJ, Reid IM, MacKinnon AD. Multistatic meteor radar observations of gravity-wave–tidal interaction over southern Australia, Atmos. Meas. Tech. 2019;4791–4812.
9. Namboothiri SP, Tsuda T, Tsutsumi M, Nakamura T, Nagasawa C, Abo M. Simultaneous observations of mesospheric gravity wave with the MU radar and a sodium lidar. J. Geophys. Res. 1996; 1057-4063.
10. Dao PD, Farley R, Tao X, Gardner C S. Lidar Observations of the Temperature Profile between 25 and 103 km: Evidence of Strong Tidal Perturbation. Geophys. Res. Lett., 1995;2825–2828.
11. Hecht JH. Instability layers and airglow imaging, Rev. Geophys; 2004.
DOI:10.1029/2003RG000131.
12. Tsuda T, Kato S, Yokoi T, Inoue T, Yamamoto M, VanZandt TE, Fukao S, Sato T. Gravity waves in the mesosphere observed with the middle and upper atmosphere radar. Radio Sci. 1990;1005 1018.
13. Nakamura T, Tsuda T, Yamamoto M, Fukao S, Kato S. Characteristics of Gravity Waves in the Mesosphere Observed With the Middle and Upper Atmosphere Radar 2. Propagation Direction. J. Geophys. Res. 1993;8911–8923.
14. Chu YH, Su CL, Larsen MF, Chao CK. First measurements of neutral wind and turbulence in the mesosphere and lower thermosphere over Taiwan with a chemical release experiment. J. Geophys. Res; 2007.
DOI:10.1029/2005JA011560
15. Fritts DC. Gravity wave saturation in the middle atmosphere: A review of theory and observations. Rev. Geophys. 1984;275 308.
16. Fritts DC, Laughman B,Wang L, Lund TS, and Collins RL. Gravity wave dynamics in a mesospheric inversion layer: 1. Reflection, trapping, and instability dynamics. Journal of Geophysical Research: Atmospheres. 2018;626–648.
17. Kim Y-J, Eckermann SD, Chun H-Y. An overview of the past, present and future of gravity-wave drag parametrization for numerical climate and weather prediction models. Atmos. Ocean. 2003;65–98.
18. Ern M, Preusse P, Gille JC, Hepplewhite CL, Mlynczak MG, Russell JM, Riese M. Implications for atmospheric dynamics derived from global observations of gravity wave momentum flux in stratosphere and mesosphere. J. Geophys. Res; 2011.
Available:https://doi.org/10.1029/2011JD0 15821
19. Chapin E, Kudeki E. Plasma wave excitation on meteor trails in the equatorial Electrojet. Geophysical Research Letters. 1994;2433-2436.
20. Reddi CR, Nair SM, Meteor trail induced backscatter in MST radar echoes. Geophys. Res. Lett. 1998;473.
21. Sugar GR. Radio propagation by reflection from meteor trails. Proc. IEEE 52. 1964; 116-136.
22. Farley DT, Ierkic HM, Fejer BG. Radar interferometry: A new technique for studying plasma turbulence in the ionosphere, J. Geophys. Res. 1981;86: 1476-1479.
23. Wang CY, Chu YH. Interferometry investigations of blob-like sporadic E plasma irregularity using the Chung-Li VHF radar. J. Atmos. Sol. Terr. Phys. 2001; 123–133.
24. Chu Y-H, Wang C-Y. Plasma structures of 3-meter type 1 and type 2 irregularities in nighttime mid-latitude sporadic E region, J. Geophys. Res. 2002;1447.
25. Gossard EE, Hooke WH. Waves in the Atmosphere, Atmospheric Infrasound and Gravity Waves—Their Generation and Propagation. Elsevier Science, Amsterdam; 1975.
26. Hedin AE et al. Revised global model of thermospheric winds using satellite and ground-based observations, J. Geophys. Res. 1991;7657-7688.
27. Close SM, Oppenheim MM, Hunt AS, Dyrud LP. Scattering characteristics of high-resolution meteor head echoes detected at multiple frequencies. J. Geophys. Res. 2002;1295.

28. Oppenheim MM, vom Endt AF, Dyrud LP. Electrodynamics of meteor trail evolution in the equatorial E-region ionosphere, Geophys. Res. Lett., 2000; 3173– 3176.

29. Pearson JM, Sharman RD. Prediction of energy dissipation rates for aviation turbulence. Part II: Nowcasting convective and nonconvective turbulence. J. Appl. Meteor. Climatol. 2017;339–351.

Peer-review history:
The peer review history for this paper can be accessed here:
http://www.sdiarticle4.com/review-history/53022